

1 **HP-LT metamorphism in Elba Island: implications for**
2 **the geodynamic evolution of inner Northern**
3 **Apennines (Italy)**

4
5 Caterina Bianco^{*,†}, Andrea Brogi^{*}, Alfredo Caggianelli^{*},
6 Giovanna Giorgetti^{**}, Domenico Liotta^{*}, Marco Meccheri^{**}

7
8 ** Dipartimento di Scienze della Terra e Geoambientali, Via Orabona 4, Bari, Italy*

9
10 *** Dipartimento di Scienze Fisiche, della Terra, ed Ambientali, Via Laterina 4, Siena, Italy*

11
12 [†] corresponding Author: caterina.bianco@uniba.it

13
14
15 **Abstract**

16
17 The inner Northern Apennines (*i.e.*, northern Tyrrhenian Sea and southern Tuscany) is
18 an Alpine chain affected by high-P metamorphic condition during its evolution.
19 Although the Elba Island is structurally located close to the Adria-Europe suture zone,
20 no evidence of high-P metamorphism has been here documented. This led to consider
21 it as a sector of the orogeny developed in a low P-context. This paper accounts for a
22 new finding of high-P and low-T metamorphism documented in metabasite rocks
23 embedded in the Cretaceous calcschist of eastern Elba Island. Mineral composition of
24 metabasite includes Gln+Cpx+Ep+Ab+Act+Qtz+Ilm±Ti-oxide±Spn and it is indicative
25 of a former equilibration in the epidote blueschist subfacies and subsequent
26 retrogression in the greenschist facies. Metamorphic peak occurred at P= 0.9-1.0 GPa

27 and $T=330-350^{\circ}\text{C}$. Tectonic discrimination using immobile elements in the metabasite
28 does not point to an oceanic setting. As a consequence, the metasedimentary
29 succession containing metabasite is interpreted as belonging to the Tuscan
30 continental domain and not to the Ligurian-Piedmont Ocean, as previously
31 interpreted. Our results have two significant implications: (i) the tectonic stacking of
32 the Elba Island units did not occur in a low-pressure context; (ii) the Elba Island is
33 now reconciled in the tectonic and metamorphic evolution of the inner Northern
34 Apennines.

35

36

37

38 1. **Introduction**

39 Northern Apennines is an eastward verging alpine belt deriving from the convergence
40 and subsequent collision between Adria microplate and Corsica-Sardinia massif,
41 believed of African and European pertinence, respectively (Molli, 2008 with references
42 therein).

43 Evidence of high-P metamorphic conditions have been detected, both in
44 metasiliciclastic rocks and metabasite, along a roughly W-E transect, from the Tuscan
45 Archipelago up to the exhumed Metamorphic Complex cropping out in southern
46 Tuscany (Fig.1).

47 Data from metasediments indicate P-T values (Fig.1) of 1.0-1.5 GPa and $\leq 350^{\circ}\text{C}$, in
48 the Tuscan Archipelago (Rossetti et al., 1999; Rossetti et al., 2001). Differently,
49 inland, the P-values are slightly lower, between 0.6 – 1.2 GPa and T is in the range
50 350–420 $^{\circ}\text{C}$ (Kligfield et al., 1986; Theye et al., 1997; Giorgetti et al., 1998; Elter and
51 Pandeli, 2002; Brogi and Giorgetti, 2012). High-P metamorphism is dated at Late
52 Oligocene-Early Miocene, on the basis of $^{40}\text{Ar}/^{39}\text{Ar}$ radiometric method (Brunet et al.
53 2000).

54 Higher and older thermobaric conditions are recorded in north-eastern Corsica where
55 P-T values up to 2 GPa and 380°C have been detected and referred to Eocene (Jolivet
56 et al., 1998; Brunet et al., 2000) and Oligocene (Rossetti et al., 2015). These data
57 are associated to westward verging thrusts (Fig.1) involving the oceanic rocks
58 presently exposed in the Alpine Corsica.

59 Thus, along the Corsica-Tuscany W-E transect (Fig.1), the Elba Island represents the
60 westernmost outcropping evidence of tectonic units verging to the east (Trevisan,
61 1950), as it is the case of the Apennine belt. In addition, and as further on described,
62 the structure of the Elba Island is characterised by the superimposition of continental
63 units over the oceanic ones, the latter already stacked on the continental successions
64 (Pertusati et al., 1993 with references).

65 This fact, therefore, enforced the interpretation that the collisional suture between the
66 European and African plates passes close to the Elba Island (Keller and Pialli, 1990;
67 Pandeli et al., 2001; Balestrieri et al., 2011). However, although studies on Si-content
68 in phengite suggested high-P occurrence (Pandeli et al., 2001), the lack of a mineral
69 assemblage confirming high-P and low-T metamorphic conditions, makes this
70 interpretation weak, thus accounting for orogenic (Late Oligocene-Early Miocene)
71 deformation developed under low-P metamorphic conditions (Keller and Coward,
72 1996; Garfagnoli et al., 2005; Musumeci and Vaselli, 2012). For this reason, Elba
73 Island resulted a distinctive case with respect to the surrounding areas, with fallouts
74 on the supposed evolution of the Northern Tyrrhenian Basin (Bonini et al., 2014).

75 In this paper we document for the first time, the occurrence of a high-P mineral
76 assemblage in metabasite interlayered to Cretaceous calcschist (Acquadolce Unit
77 *Auctt.*). We conclude that high-P and low-T metamorphism affected the whole tectonic
78 pile of the Elba Island, at least up to the Early Burdigalian, as suggested by Deino et
79 al. (1992) age measurements, thus reconciling the evolution of the Elba Island with
80 the Northern Apennines.

81

82

83 **2. Geological framework**

84 The geodynamic process leading to the Northern Apennines orogenesis determined
85 the eastward stacking of several tectonic units belonging to oceanic and continental
86 paleogeographic domains. These are: (a) the Ligurian Units, consisting of remnants of
87 Jurassic oceanic crust, with the Jurassic-Cretaceous cover (Ligurian Units) and
88 Cretaceous-Oligocene turbidites (Sub-Ligurian Units); these units were thrust
89 eastwards over the Tuscan Nappe during Late Oligocene-Early Miocene times; (b) the
90 inner Tuscan Domain, made up of a complete sedimentary succession of evaporitic,
91 platform, pelagic and foredeep environments, ranging in age from Late Trias to Early
92 Miocene. During Early Miocene, the Tuscan succession was internally deformed and
93 detached from its substratum along the late Triassic evaporite level, giving rise to the
94 Tuscan Nappe. This latter stacked over the external Tuscan domain, that was
95 deformed in isoclinal folds and duplex structures, under metamorphic conditions from
96 the blueschist to the greenschist facies (Carmignani and Kligfield, 1990; Carmignani
97 et al., 1994; Jolivet et al., 1998; Rossetti et al., 2002; Molli, 2008; Brunet et al.,
98 2000; Brogi and Giorgetti, 2012). During Early-Middle Miocene (Jolivet et al., 1990;
99 Carmignani et al., 1995; Brunet et al., 2000) the tectonic framework changed and an
100 eastward migrating extension affected the inner Northern Apennines (i.e., northern
101 Tyrrhenian Sea and southern Tuscany). Extension continuously developed through
102 time, although two main events can be distinguished (Barchi, 2010 with references
103 therein). The first one, occurred during Miocene, determined the lateral segmentation
104 of the more competent levels within the previously stacked tectonic units and the
105 consequent superimposition of the Ligurian Units (at the top of the tectonic pile) on
106 the deeper basal detachment levels. These are within the late Triassic evaporite and
107 the Palaeozoic phyllite (Bertini et al., 1991; Baldi et al., 1994), and, consequently, the

108 stair-case geometry of the faults gave rise to bowl-shaped structural depressions
109 where Langhian-Messinian marine to evaporitic and continental sediments deposited
110 (Brogi and Liotta, 2008). The second extensional event (Pliocene-Quaternary)
111 determined normal faults crosscutting the previously developed compressional and
112 extensional structures, thus defining tectonic depressions filled up by Pliocene to
113 Quaternary marine and continental sediments (Bossio et al., 1993). Since Late
114 Miocene, extension is accompanied by anatectic magmatism with minor mantle
115 contribution (Peccerillo, 2003).

116

117 **2.1. Elba Island geological framework**

118 Integrating previous papers (Trevisan, 1950; Keller and Piali, 1990; Pertusati et al.,
119 1993; Bortolotti et al., 2001 with references therein) with the data here further on
120 illustrated, we distinguish seven main tectonic units, belonging both to continental
121 and oceanic environments and forming the tectonic pile of the Elba Island (Fig.2). The
122 deeper outcropping continental unit (continental unit 1, Fig.3) is made up of early
123 Carboniferous micaschist (Musumeci et al., 2011) and its Triassic-Jurassic siliciclastic
124 and carbonatic cover (Porto Azzurro Unit, in Pandeli et al., 2005).

125 The 2nd continental unit (Fig.3) is made up of a complete succession of metamorphic
126 rocks consisting of middle Ordovician porphyroids (Ortano porphyroids, Musumeci et
127 al., 2011) above which Mesozoic continental to marine metasediments crop out
128 (Duranti et al., 1992). The latter are late Triassic to Jurassic metacarbonates,
129 calcschist and metaradiolarite passing to a Cretaceous succession made up of
130 calcschist and phyllite with levels of metasiltstone and metasandstone. Calcschist
131 represents the base of the succession and contains discontinuous lenses of metabasite
132 (Fig.3), the main focus of this paper. The third continental unit (Fig.3) consists of low-
133 grade metamorphic rocks including late Carboniferous phyllite, overlain by Triassic
134 continental quartzite and phyllite, marine ?Triassic-?Jurassic marble and by the

135 Cretaceous-Oligocene carbonatic and terrigenous metasedimentary succession
136 (Bortolotti et al., 2001). Finally, the fourth continental unit (Fig.3) is related to the
137 Tuscan Nappe, composed of late Triassic, locally vacuolar and fragmented calcareous
138 dolostone, overlain by Jurassic marine carbonate and Cretaceous-Oligocene
139 calcareous and marly pelagic sediments. The oceanic unit 1 (Fig.3) is interposed
140 between the second and the third continental units by means of out-of-sequence
141 thrust (Keller and Pialli, 1990; Pertusati et al., 1993; Keller and Coward, 1996)
142 referred to Early Burdigalian (Deino et al., 1992; Pertusati et al., 1993). This unit is a
143 tectonic slice made up of Jurassic ophiolite. Finally, the oceanic units 2 and 3 (Fig.3)
144 consist of remnants of the Jurassic ophiolite, Jurassic radiolarite and Cretaceous-
145 Eocene calcareous and terrigenous sediments, with levels of ophiolitic breccias. After
146 the stacking of the tectonic pile, the Elba Island was affected by Miocene extensional
147 structures and magmatism (Fig.2), giving rise to the emplacement of Monte Capanne
148 (about 7.0 Ma, Westerman et al., 2004), and Porto Azzurro (about 6 Ma, Maineri et al.
149 2003 and Musumeci et al. 2011) laccolith-pluton-dyke granitic complexes (Dini et al.
150 2002), respectively located to the West and East sides of the Island (Fig.2).
151 Regionally, magma emplacement and cooling (Caggianelli et al., 2014) determined
152 thermo-metamorphic aureolas (Barberi and Innocenti, 1965; Duranti et al., 1992;
153 Rossetti et al., 2007) and low-P mineral assemblage resetting the older metamorphic
154 paragenesis related to the collisional event (Duranti et al., 1992; Pertusati et al.,
155 1993). Moreover, a diffuse hydrothermalism determined Fe-ore deposits (Tanelli,
156 1983; Tanelli et al., 2001), particularly in the Eastern Elba Island. In this framework,
157 it was surprising to find relic high-pressure metamorphic paragenesis still preserved in
158 metabasite lithons, embedded in the calcshist of the Continental unit 2 (Fig.3).

159

160 **3 - Rock fabric**

161 The sampling area (Fig.4 and Fig. 5A) is structurally located in the lower part of the
162 Cretaceous succession of the continental unit 2 (Fig.3). Here, lenses of metabasite,
163 from few cm to about 2 m thick (Fig. 5B), are embedded in calcschist, mainly along
164 the main schistosity, gently NW-dipping (Fig.5C-5D). The metabasite is laterally
165 segmented at different scales (Fig. 5E-H), indicating the pervasiveness of the
166 deformation. The rock fabric is characterized by the presence of porphyroclasts of
167 mafic minerals within a chloritic matrix (Fig.5I) and by S/C structures.

168 In calcschist, the main foliation, generally parallel to S_0 (Fig.5), is locally deformed by
169 tight and isoclinal folds with $\approx 304/30$ plunging hinge lines (Fig. 6A-B). These folds,
170 characterised by the lack of an axial plane foliation, account for thermal conditions
171 favoring plastic behavior. The stretching lineation is well defined by elongated calcite
172 crystals, NW-SE trending (Fig. 6C). The mineral association (Fig. 6D) on main
173 schistosity is made up of $Cal+Dol+Qtz+Bt+Ms+Chl\pm Ti-FeOxides\pm Ab\pm Ap\pm Ep$ (mineral
174 abbreviations after Kretz, 1983 and Bucher and Frey, 1994). Close to this study
175 outcrop (Fig.4), few tens of meter southwards, muscovite on the main foliation has
176 been dated through $^{40}Ar/^{39}Ar$ method at 19.68 ± 0.15 Ma (Deino et al., 1992). A new
177 deformation episode affected the previous structures, determining local open and SE-
178 verging folds.

179

180 **4. evidence of HP metamorphism**

181 Main evidence of high-P and low-T metamorphic conditions are from the metabasite
182 embedded in the calcschist. The nature of the parental material of the metabasite was
183 ascertained by XRF analyses for three rock samples. Results in Table 1 indicate low
184 contents in SiO_2 (down to 43.60 wt. %) and K_2O (down to 0.56 wt. %) and high
185 contents in MgO (up to 9.92 wt. %) and Na_2O (up to 3.49 wt. %). Finally, a wide
186 variation in CaO (from 6.28 to 12.36 wt. %) and elevated values of L.O.I. (up to 9.25
187 wt. %) can be noted. Classification of these rocks was performed by the Winchester

188 and Floyd (1977) diagram based on immobile elements distribution, as modified by
189 Pearce (1996; 2014). In Fig. 7, the analysed rocks are in the field of basalt, near the
190 boundaries with the andesite/basaltic andesite and alkali basalt fields, resulting
191 different from N-MORB and the well known ophiolitic lavas of Troodos and Semail
192 (Pierce, 2014). The mineralogical composition of the metabasite includes
193 $Gln+Cpx+Ep+Ab+Act+Qtz+Ilm\pm Ti\text{-oxide}\pm Spn$. It is indicative of former equilibration
194 in the epidote blueschist subfacies (Evans, 1990) and later retrogression in the
195 greenschist facies. Metabasite has a fine grain size and sometimes a mylonitic fabric
196 characterized by clinopyroxene porphyroclasts set in a matrix mainly made up of
197 glaucophane and epidote + chlorite. Clinopyroxene porphyroclasts are typically
198 rounded and fragmented (Fig.8A-C), probably representing relics of former magmatic
199 diopside and augite. They usually appear brownish and rare portions apparently
200 unaffected by alteration characterized by bright interference colors. Elongated
201 glaucophane crystals, recognizable for the pale lavender color shades, are
202 preferentially oriented along the main foliation (Fig.8C) and wrap around
203 clinopyroxene porphyroclasts (Fig.8D). Glaucophane is present also in the strain
204 shadows and in the fractures of the stretched porphyroclasts (Fig.8A-B). Epidote
205 occurs in minor amounts with respect to glaucophane and is represented by small
206 grains, occasionally with lamellar twinning, of both clinozoisite and pistacite. It is
207 occasionally zoned with clinozoisite cores and pistacite rims, a texture reflecting the
208 transition to lower pressure conditions. Ilmenite and, if present, Ti-oxide, are
209 scattered throughout the rock, showing a variable grain size. Sometimes, ilmenite can
210 be surrounded by sphene (Fig. 8E). Rock portions characterized by the abundance of
211 chlorite, epidote, sphene and Ti-oxide, when glaucophane and clinopyroxene relics are
212 scarce (Fig.8E), indicate that later retrogression was non-pervasive and took place in
213 the greenschist facies (Fig.8E). Another common textural evidence of retrogression is

214 represented by albite blasts enclosing glaucophane and by the presence of
215 calcite±actinolite veins crosscutting the main foliation (Fig. 8F).

216 In Table 2 microprobe analyses and structural formulae of selected minerals,
217 representative of the metabasite assemblage in sample C19, are provided. We focus
218 hereafter on those mineral phases (*i.e.*: glaucophane, clinopyroxene, epidote) used to
219 constrain the P-T conditions of the epidote blueschist subfacies metamorphism.

220 Blue-amphibole nomenclature was defined according to Leake (1997) by using the
221 software Probe-Amph (Tindle et al., 1994). It was established that all Na-amphibole
222 analyses can be attributed to glaucophane (Fig.9A). Content in glaucophane molecula
223 X_{Gln} , calculated as $Al^{VI}/[Fe^{3+} + Al^{VI}]$ ranges from 0.65 to 0.86. Ca-amphibole analyses
224 are related to Fe-actinolite with average X_{Mg} of 0.78.

225 Clinopyroxene nomenclature was defined following Morimoto et al. (1988) and using
226 the PX-NOM software (Sturm, 2002). Clinopyroxene porphyroclasts surrounded by
227 glaucophane fibres can be classified in most cases as omphacite and secondly as
228 aegirine-augite (Fig. 9B). For these types, content in jadeite molecula ranges from
229 0.24 to 0.33, indicating their involvement in the high-pressure metamorphic reactions.

230 However, a smaller number of analyses, generally pertaining to isolated
231 porphyroclasts (Fig.9C) without external glaucophane fibres, can be classified as
232 diopside (average X_{Mg} =0.80) and, in one case, as augite (X_{Mg} =0.65). Therefore, they
233 can be ascribed to magmatic clinopyroxene relics. Epidote is represented by both
234 clinozoisite- and pistacite-rich terms. The content in pistacite molecula (X_{Ps}) has been
235 calculated by $Fe/[(Al-4)+Fe]$ on the basis of $\Sigma O = 25$. It results that clinozoisite is
236 characterized by a minimum value of $X_{Ps} = 0.09$ and pistacite by a maximum value of
237 $X_{Ps} = 0.82$. Interestingly, in the matrix of two metabasites, microanalyses allowed to
238 recognize the presence of anorthite with composition very close to pure calcic
239 plagioclase end-member (Table 2). Anorthite was probably generated from a former
240 lawsonite in response to the later heating produced at low-P conditions by the

241 emplacement of the Porto Azzurro monzogranite pluton, as an effect of the reaction
242 lawsonite=anorthite+H₂O.

243 The mineral compositional data from metabasite were used for a preliminary
244 estimation of the P-T conditions in the epidote-blueschist metamorphic subfacies. To
245 this end, we considered the pyroxene porphyroclasts with omphacite composition
246 (max X_{Jd} = 0.33) and glaucophane (max X_{Gln} = 0.86).

247 We firstly used the approach described by Sturm (2002) based on the albite =jadeite
248 + quartz equilibrium, experimentally determined by Holland (1980). This calibration
249 was obtained for temperatures higher than blueschist facies but, according to Sturm
250 (2002), extrapolation to lower temperatures produces small uncertainties in P values
251 and can provide acceptable preliminary estimates. Therefore, considering the
252 maximum content of jadeite molecula (X_{Jd}=0.33) in omphacite, pressure values
253 ranging from 0.95 to 1.10 GPa are obtained if the field of the epidote blueschists
254 subfacies by Tsujimori and Ernst (2013) is considered (Fig.10). Indeed, the relatively
255 low content of epidote in the metabasite and the suspected former presence of
256 lawsonite, now replaced by anorthite, point to a peak P-T condition in the
257 neighbourhood of the transition from lawsonite- to epidote-blueschist subfacies.
258 According to Zhang et al. (2009), blueschists of NW China crossed this transition
259 during subduction at temperatures close to 350 °C. In Fig.10 the isopleth related to
260 the observed maximum content in jadeite molecula meets the transition line between
261 the two subfacies at a T of c. 330 °C, corresponding to a pressure of c. 0.95 GPa.
262 Lower P estimates (Fig.10) are obtained on the basis of the Na-amphibole
263 composition. By following the calibration of Maruyama et al. (1986) and by plotting
264 the isopleth related to the maximum content in glaucophane molecula in the field of
265 epidote blueschist subfacies, a value of pressure slightly above 0.7 GPa is estimated.
266 This result may indicate that, after the peak pressure condition, glaucophane re-
267 equilibrated in a later stage during the exhumation.

268 A confirmation of the high-pressure metamorphic event was obtained from SEM-EDS
269 analyses revealing the presence of white mica (Fig. 11A) with an elevated content in
270 celadonite molecula ($X_{\text{Cel}}=0.5$ and $\text{Si}=3.5$ a.p.f.u.) in metabasite sample RMT3 (Table
271 3). However, although it accounts for high-P conditions, the lack of a limiting mineral
272 assemblage in equilibrium with phengite (*i.e.*: K-feldspar, quartz, Mg/Fe silicates)
273 precludes quantifying pressure by a geobarometric approach.

274 Another indication in favor of the high-pressure metamorphism comes from a
275 phengite-bearing quartzite (sample RIO6B) in the Torre Giove locality (Fig. 2, 11B and
276 Table 3). The main schistosity is defined by $\text{Qtz}+\text{Ms}+\text{Kln}\pm\text{Cal}\pm\text{Fe-Ti oxide}$. In some
277 cases, detrital grains of white mica are surrounded by aggregates of newly-formed
278 flakes of phengite (Fig. 11B) with Si content of about 3.5 a.p.f.u. (Table 3).

279

280

281 **5. Discussion and Conclusions**

282 The metasedimentary succession where we have found metabasite, has been
283 differently interpreted through time. According to Trevisan (1950), Barberi et al.
284 (1969), Perrin (1975) and Keller and Piali (1990), it is considered as part of the
285 sedimentary succession belonging to the Tuscan Domain. Differently, Duranti et al.
286 (1992) and Pertusati et al. (1993) interpreted the ophiolite slice (*i.e.* the oceanic unit
287 1 in Fig. 3) and the underlying metasedimentary succession, where the study
288 metabasite is embedded, as belonging to the same overturned Jurassic-Cretaceous
289 oceanic succession of the inner Ligurian Domain (Pertusati et al., 1993). This unit was
290 later affected by contact metamorphism during the emplacement of the Porto Azzurro
291 monzogranite (Duranti et al., 1992). Pandeli et al. (2001) followed this interpretation
292 and suggested that this succession can be related to the Piedmont Ocean sedimentary
293 evolution.

294 Our data indicate that the composition of the metabasite rocks (Fig.7) is not
295 compatible with an oceanic setting, *i.e.* the Ligurian-Piedmont Ocean. Thus, we
296 sustain that the hosting metasediments cannot be related to the sedimentary
297 succession of the ophiolite slice (oceanic unit 1 in Fig. 3). The latter instead is
298 tectonically located above the calcschist (Fig.2). As a consequence, and as already
299 proposed by the previously cited Authors, the metasedimentary succession under
300 discussion should be linked to the Tuscan domain (Fig.3).

301 Mineral association and P-T conditions indicate an equilibration of the metabasite in
302 the epidote blueschist subfacies with a pressure peak of 0.9-1.0 GPa. Metamorphic
303 studies (Fig.1) carried out in the inner Northern Apennines indicate an eastward
304 decrease of pressure (Rossetti et al. 2002 with references therein), from 1.3-1.6 GPa
305 (Gorgona and Giglio Islands, Fig.1) to 0.8-1.0 GPa (southern Tuscany), as obtained on
306 metasediments with Fe-Mg silicates (Giorgetti et al., 1998; Rossetti et al, 1999;
307 Rossetti et al., 2001; Agard et al., 2000).

308 A comparison between P-values obtained for metasediment and metabasite
309 parageneses from other localities of inner Northern Apennines (Fig.1), indicates that
310 the metamorphic peak in metabasites is encompassed between 0.6 and 0.8 GPa (T=
311 275-350°C). Instead, P-values obtained from metasediments range from 0.8 to 1.5
312 GPa (T=350-420°C) in six out of seven localities. Thus it can be inferred that
313 metabasites usually provide peak estimates lower than metasediments.

314 Although in the Elba Island pressure estimate is slightly higher (P=0.9-1.0 GPa;
315 T=330-350°C) than those obtained for the other metabasites, we interpret all the
316 barometric values in the same tectono-metamorphic framework of the inner Northern
317 Apennines. On this basis, the result provided by the Elba Island metabasite has two
318 significant implications: (i) the tectonic stacking of the Elba Island units did not occur
319 in a low-P context, as supposed by Pertusati et al. (1993) and, more recently, by
320 Musumeci and Vaselli (2012); (ii) the Elba Island is now reconciled in the tectonic and

321 metamorphic evolution of the Northern Apennines. Furthermore, it results that its
322 stratigraphic and metamorphic evolution is significantly similar to the one described
323 for the Gorgona Island, suggesting that the interpretation of the Gorgona calcschist as
324 a part of the Piedmont Ocean (Capponi et al., 1990; Pandeli et al., 2001; Rossetti et
325 al., 2001) should be revised.

326 Finally, considering reasonable that the high content of Si in phengite from the Monte
327 Giove area is a further evidence of high-P conditions, it derives that continental units
328 2 and 3 (Fig. 3) have been affected by high P-metamorphism too. Consequently, it
329 can be inferred that also the oceanic unit 1, interposed between the continental unit 2
330 and 3 (Fig.3 and 4), underwent metamorphism in high-P conditions. The absence of a
331 corresponding paragenesis, is probably an effect of the thermal perturbation produced
332 by the emplacement of the Porto Azzurro monzogranite (Pertusati et al., 1993;
333 Bortolotti et al., 1994).

334 As it regards the timing of metamorphism, we have in the area two different
335 radiometric ages: Brunet et al. (2000) dated muscovite on the main schistosity of
336 calcschist cropping out in the Gorgona Island (Fig.1), obtaining 25.5 ± 0.3 Ma by
337 $^{40}\text{Ar}/^{39}\text{Ar}$ geochronology; by the same method, Deino et al. (1992) dated the
338 muscovite, grown on the main schistosity of the calcschist of the Elba Island (Fig.4),
339 providing a radiometric age of 19.68 ± 0.15 Ma. Assuming that the study metabasite
340 and hosting calcschist record the same deformational event and considering that both
341 glaucophane in metabasite, and white mica in calcschist, are syn-kynematic, we
342 suggest that the radiometric ages are indicative for the high-P metamorphic event.
343 We can therefore assess that the high-P conditions occurred during the late
344 Oligocene-early Burdigalian time interval.

345

346 **ACKNOWLEDGMENTS**

347 The research leading to these results has received funding from the European

348 Community's Seventh Framework Programme under grant agreement No. 608553
349 (Project IMAGE).

350

351

352 **REFERENCES**

353

354 Agard, P., Goffé, B., Touret, J.L.R., Vidal, O., 2000. Retrograde fluid evolution in
355 blueschist-facies metapelites (Schistes lustrés unit, Western Alps). *Contrib.*
356 *Mineral. Petr.* 140, 296–315.

357 Baldi, P., Bertini, G., Cameli, G.M., Decandia, F.A., Dini, I., Lazzarotto, A., Liotta, D.,
358 1994. Tettonica distensiva post-collisionale nell'area geotermica di Larderello
359 (Toscana meridionale). *Studi Geologici Camerti Spec* 1, 183–193.

360 Balestrieri, M.L., Pandeli, E., Bigazzi, G., Carosi, R., Montomoli, C., 2011. Age and
361 temperature constraints on metamorphism and exhumation of the syn-orogenic
362 metamorphic complexes of Northern Apennines, Italy. *Tectonophysics*, 509, 254-
363 271.

364 Barberi, F., Dallan, L., Franzini, M., Giglia, G., Innocenti, F., Marinelli, G., Raggi, R.,
365 Ricci, C.A., Squarci, P., Taffi, L., Trevisan, L., 1969. Note illustrative della Carta
366 Geologica d' Italia alla scala 1:100.000, Foglio 126 (Isola d'Elba). *Serv. Geol.*
367 *d'It.*, 32 pp.

368 Barberi, F., Innocenti, F., 1965. Le rocce cornubianitico-calcaree dell'anello
369 termometamorfico del Monte Capanne (Isola d'Elba). *Atti Soc. Tosc. Sci. Nat.*,
370 *Mem.*, Ser. A 72, 306-398.

371 Barchi, M.R., 2010. The Neogene-Quaternary evolution of the Northern Apennines:
372 crustal structure, style of deformation and seismicity. In: Beltrando, M.,
373 Peccerillo, A., Mattei, M., Conticelli, S., Doglioni, C. (Eds.): *The Neogene-
374 Quaternary evolution of the Northern Apennines: crustal structure, style of*

375 deformation and seismicity. *Journ. Virt. Explorer* 36,
376 doi:10.3809/jvirtex.2009.00220.

377 Bertini, G., Cameli, G.M., Costantini, A., Decandia, F.A., Di Filippo, M., Dini, I., Elter,
378 F.M., Lazzarotto, A., Liotta, D., Pandeli, E., Sandrelli, F., Toro, B., 1991.
379 Struttura geologica fra i monti di Campiglia e Rapolano Terme (Toscana
380 meridionale): stato attuale delle conoscenze e problematiche. *Studi Geol.*
381 *Camerti* 1, 155–178.

382 Bonini, M., Sani, F., Stucchi, E.M., Moratti, G., Benvenuti, M., Menanno, G., Tanini, C.,
383 2014. Late Miocene shortening of the Northern Apennines back-arc. *J.*
384 *Geodynamics* 74, 1-31.

385 Bortolotti, V., Cellai, D., Martin, S., Principi, G., Tartarotti, P., Vaggelli, G., 1994.
386 Ultramafic rocks from the eastern Elba island ophiolites (Tyrrhenian Sea, Italy).
387 *Mem. Soc. Geol. It.* 48, 195-202.

388 Bortolotti, V., Fazzuoli, M., Pandeli, F., Principi, G., Babbini, A., Corti, S., 2001.
389 Geology of Central and Eastern Elba Island, Italy. *Ofioliti* 26, 97-150.

390 Bossio, A., Costantini, A., Lazzarotto, A., Liotta, D., Mazzanti, R., Mazzei, R.,
391 Salvatorini, G.F., Sandrelli, F., 1993. Rassegna delle conoscenze sulla stratigrafia
392 del Neoauctono toscano. *Mem. Soc. Geol. It.* 49, 17–98.

393 Brogi, A., Giorgetti, G., 2012. Tectono-metamorphic evolution of the siliciclastic units
394 in the Middle Tuscan Range (inner Northern Apennines): Mg–carpholite bearing
395 quartz veins related to syn-metamorphic syn-orogenic foliation. *Tectonophysics*,
396 526–529 (2012) 167–184.

397 Brogi, A., Liotta, D., 2008. Highly extended terrains, lateral segmentation of the
398 substratum, and basin development: the Middle–Late Miocene Radicondoli Basin
399 (inner northern Apennines, Italy). *Tectonics* 27. doi:10.1029/2007TC002188 TC
400 5002.

- 401 Brunet, C., Monie, P., Jolivet, L., Cadet, J.P., 2000. Migration of compression and
402 extension in the Tyrrhenian sea, insights from $^{40}\text{Ar}/^{39}\text{Ar}$ ages on micas along a
403 transect from Corsica to Tuscany. *Tectonophysics* 321, 127–155.
- 404 Bucher, K., Frey, M., 1994. *Petrogenesis of metamorphic rocks*. Springer-Verlag,
405 Berlin, 318 pages.
- 406 Butler, R.W.H., 1987. Thrust sequences. *Journ. Geol. Soc. London* 144, 619-634.
- 407 Caggianelli, A., Ranalli, G., La Vecchia, A., Liotta, D., Dini, A., 2014. Post-
408 emplacement thermo-rheological history of a granite intrusion and surrounding
409 rocks: the Monte Capanne pluton, Elba Island, Italy. From: Llana-Fúnez, S.,
410 Marcos, A. & Bastida, F. (eds) *Deformation Structures and Processes within the*
411 *Continental Crust*. Geological Society, London, Special Publications, 394, 129-
412 143.
- 413 Capponi, G., Giammarino, S., Mazzanti, R., 1990. Geologia e morfologia dell'Isola di
414 Gorgona. *Quad. Mus. Stor.Nat. Livorno* 11, 115-137
- 415 Carmignani, L., Decandia, F.A., Disperati, L., Fantozzi, P.L., Lazzarotto, A., Liotta, D.,
416 Meccheri, M., 1994. Tertiary extensional tectonics in Tuscany (Northern
417 Apennines, Italy). *Tectonophysics* 238, 295–315.
- 418 Carmignani, L., Decandia, F.A., Disperati, L., Fantozzi, P.L., Lazzarotto, A., Liotta, D.,
419 Oggiano, G., 1995. Relationships between the Sardinia-Corsica-Provencal
420 Domain and the Northern Apennines. *Terranova* 7, 128–137.
- 421 Carmignani, L., Kligfield, R., 1990. Crustal extension in the Northern Apennines: the
422 transition from compression to extension in the Alpi Apuane core complex.
423 *Tectonics*, 9, 1275-1303.
- 424 Chemenda, A.I., Mattauer, M., Malavieille, J., Bokun, A., 1995. A mechanism for
425 syncollisional rock exhumation and associated normal faulting: results from
426 physical modelling. *Earth Plan. Sc. Lett.* 132, 225–232.
- 427 Crawford, W.A., Fyfe, W.S., 1965. Lawsonite equilibria. *Am. J. Sci.* 263, 262-270.

- 428 Deino, A., Keller, J.V.A., Minelli, G., Pialli, G., 1992. Datazioni $^{39}\text{Ar}/^{40}\text{Ar}$ del
429 metamorfismo dell'Unità di Ortano-Rio Marina (Isola d'Elba): risultati preliminari.
430 Studi Geol. Camerti 1, 187–192.
- 431 Dini, A., Innocenti, F., Rocchi, S., Tonarini, S., Westerman, D.S., 2002. The magmatic
432 evolution of the Late Miocene laccolith–pluton–dyke granitic complex of Elba
433 Island, Italy. Geol. Mag. 139, 257–279.
- 434 Duranti, S., Palmieri, R., Pertusati, P.C., Ricci, C.A., 1992. Geological evolution and
435 metamorphic petrology of the basal sequences of eastern Elba (Complex II). Acta
436 Vulcanologica 2, 213-229.
- 437 Elter FM., Pandeli E. 2002. The HP-LP meta-ophiolitic unit and Verrucano of the Cala
438 Grande Area in the Argentario Promontory (southern Tuscany, Italy): structural
439 metamorphic evolution and regional considerations. Ofioliti, 27(2), 91-102.
- 440 Evans, B.W., 1990. Phase relations of epidote-blueschists. Lithos 25, 3–23.
- 441 Garfagnoli, F., Menna, F., Pandeli, E., Principi, G., 2005. The Porto Azzurro Unit (Mt.
442 Calamita promontory, south-eastern Elba Island, Tuscany): stratigraphic,
443 tectonic and metamorphic evolution. Boll. Soc. Geol. It. 3, 119-138.
- 444 Giorgetti, G., Goffé, B., Memmi, I., Nieto, F., 1998. Metamorphic evolution of
445 Verrucano metasediments in northern Apennines: new petrological constraints.
446 Eur. Journ. Miner. 10, 1295–1308.
- 447 Holland, T.J. B., 1980. The reaction albite=jadeite + quartz determined
448 experimentally in the range 600°-1200°C. Am. Miner. 65, 129-134.
- 449 Jolivet, L., Dubois, R., Fournier, R., Goffé, B., Michard, A., Jourdan, C., 1990. Ductile
450 extension in alpine Corsica. Geology 18, 1007–1010.
- 451 Jolivet, L., Faccenna C., Goffé, G., Burov, E., Agard, P., 2003. Subduction tectonics
452 and exhumation of high-pressure metamorphic rocks in the mediterranean
453 orogens. Am. J. Sci. 303, 353-409.

454 Jolivet, L., Goffé, B., Truffert-Luxey, C., Patriat, M., Bonneau, M. 1996. Miocene
455 detachment in Crete and exhumation P-T-t paths of high-pressure metamorphic
456 rocks. *Tectonics* 15, 1129-1153.

457 Jolivet, L., Faccenna, C., Goffé, B., Mattei, M., Rossetti, F., Brunet, C., Storti, F.,
458 Funiciello, R., Cadet, J.P., D'Agostino, N., Parra, T., 1998. Midcrustal shear zones
459 in postorogenic extension: example from the northern Tyrrhenian Sea. *J.*
460 *Geophys. Res.* 103 (B6), 12123–12160.

461 Keller, J.V.A., Pialli, G., 1990. Tectonics of the island of Elba: a reappraisal. *Boll. Soc.*
462 *Geol. It.* 109, 413–425.

463 Keller, JVA, Coward, MP., 1996. The structure and evolution of the Northern
464 Tyrrhenian Sea. *Geol. Magazine* 133, 1-16.

465 Kligfield, R., Hunziker, J., Dallmayer, R.D., Schamel, S., 1986. Dating of deformation
466 phases using K-Ar and $^{40}\text{Ar}/^{39}\text{Ar}$ techniques: results from the Northern
467 Apennines. *J. Struct. Geol.* 8, 781-798.

468 Kretz, R., 1983. Symbols for rock-forming minerals. *Am. Mineral.* 68, 277-279.

469 Leake, BE., Woolley, AR., Arps, C.E.S., Birch, W.D., Gilbert, M.C., Grice, J.D.,
470 Hawthorne, F.C., Kato, A., Kisch, H.J, Krivovichev, V.G., Linthout, K., Laird, J.,
471 Mandarino, J.A., Maresch, W.V., Nickel, E.H., Rock, N.M.S., Schumacher, JC;
472 Smith, DC; Stephenson, N.C.N., Ungaretti, L., Whittaker, E.J.W., Guo, Y.Z.,
473 1997. Nomenclature of amphiboles: Report of the subcommittee on amphiboles
474 of the International Mineralogical Association, commission on new minerals and
475 mineral names. *Am. Mineral.* 82, 1019-1037.

476 Maresch, W.V., 1977. Experimental studies on glaucophane: an analysis of present
477 knowledge. *Tectonophysics* 43, 109-125.

478 Maruyama, S., Cho, M., Liou, J.G., 1986. Experimental investigations of blueschist-
479 greenschist transition equilibria: Pressure dependence of Al_2O_3 contents in sodic
480 amphiboles- a new geobarometer. *Geol. Soc. Am. Memor* 164, 1-16.

- 481 Maineri, C., Benvenuti, M., Costagliola, P. Dini, A., Lattanzi, P., Ruggieri, G., Villa,
482 I.M., 2003. Sericitic alteration at the La Crocetta deposit (Elba Island, Italy):
483 interplay between magmatism, tectonics and hydrothermal activity. *Mineralium*
484 *Deposita* 38, 67-86.
- 485 Molli, G., 2008. Northern Apennine–Corsica orogenic system: an updated overview.
486 *Geol. Soc. London, Spec. Publ.* 298, 413–442.
- 487 Morimoto, N., Fabries, J., Ferguson, A.K., Ginzburg, R.M., Seifert, F., Zussman, J.,
488 Aoki, K., Gottardi, G., 1988. Nomenclature of Pyroxenes. *Am. Mineral.* 73, 1123-
489 1133.
- 490 Musumeci, G., Mazzarini, F., Tiepolo, M., Di Vincenzo, G., 2011. U-Pb and ^{40}Ar - ^{39}Ar
491 geochronology of Palaeozoic units in the Northern Apennines: determining
492 protolith age and alpine evolution using the Calamita Schist and Ortano
493 Porphyroids. *Geol. J.* 46, 288–310.
- 494 Musumeci, G., Vaselli, L., 2012. Neogene deformation and granite emplacement in the
495 metamorphic units of northern Apennines (Italy): Insights from mylonitic
496 marbles in the Porto Azzurro pluton contact aureole (Elba Island). *Geosphere* 8,
497 470–490.
- 498 Pandeli, E., Puxeddu, M., Ruggieri, G., 2001. The metasiliciclastic-carbonate sequence
499 of the Acquadolce Unit (eastern Elba Island): new petrographic data and
500 palaeogeographic interpretation. *Ofioliti* 26, 207-218.
- 501 Pearce, J.A., 1996. A user's guide to basalt discrimination diagrams. In: Wyman, D. A.
502 (Eds.), *Trace element geochemistry of volcanic rocks; applications for massive*
503 *sulphide exploration*. *Geol. Ass. Canada, Short Course Notes* 12, 79-113.
- 504 Pearce, J.A., 2014. Immobile elements finger printing of ophiolite. *Elements* 10, 101-
505 108.
- 506 Peccerillo, A., 2003. Plio-Quaternary magmatism in Italy. *Episodes* 26, 222–226.

- 507 Perrin, M., 1975. L'île d'Elbe et la limite Alpes-Apennin: données sur la structure
508 géologique et l'évolution tectogénétique de l'Elbe Alpine et de l'Elbe Apennine.
509 Boll. Soc. Geol. It. 94, 1929-1955.
- 510 Pertusati, P., Raggi, G., Ricci, C.A., Duranti, S., Palmeri, R., 1993. Evoluzione post-
511 collisionale dell'Elba centro-orientale. Mem. Soc. Geol. It. 49, 297-312.
- 512 Rossetti, F., Faccenna, C., Jolivet, L., Funiciello, R., Tecce, F., Brunet, C., 1999. Syn-
513 versus post-orogenic extension: the case study of Giglio Island (Northern
514 Tyrrhenian Sea, Italy). Tectonophysics 304, 73-92.
- 515 Rossetti, F., Faccenna, C., Jolivet, L., Funiciello, R., Goffè, B., Tecce, F., Brunet, C.,
516 Monié, P., Vidal, O., 2001. Structural signature and exhumation P-T-t path of
517 the Gorgona blueschist sequence (Tuscan Archipelago, Italy). Ofioliti 26, 175-
518 186.
- 519 Rossetti, F., Faccenna, C., Jolivet, L., Goffé, B., Funiciello, R., 2002. Structural
520 signature and exhumation P-T-t paths of the blueschist units exposed in the
521 interior of the Northern Apennine chain, tectonic implications. Boll. Soc. Geol. It.
522 1, 829-842.
- 523 Rossetti, F., Glodny, J., Theye, T., Maggi, M., 2015. Pressure-Temperature-
524 deformation-time of the ductile Alpine shearing in Corsica: from orogenic
525 construction to collapse, LITHOS, doi: 10.1016/j.lithos.2015.01.011
- 526 Rossetti, F., Tecce, F., Billi, A., Brillì, M., 2007. Patterns of fluid flow in the contact
527 aureole of the Late Miocene Monte Capanne pluton (Elba Island, Italy): the role
528 of structures and rheology. Contrib. Mineral. Petrol. 153, 743-760.
- 529 Sturm, R., 2002. PX-NOM—an interactive spreadsheet program for the computation of
530 pyroxene analyses derived from the electron microprobe. Computers &
531 Geosciences 28, 473-483.
- 532 Tanelli, G., 1983. Mineralizzazioni metallifere e minerogenesi della Toscana. Mem.
533 Soc. Geol. It. 25, 91-109.

- 534 Tanelli, G., Benvenuti, M., Costagliola, P., Dini, A., Lattanzi, P., Manieri, C., Mascaro,
535 I., Ruggieri, G., 2001. The iron mineral deposits of Elba Island: state of the art.
536 *Ofioliti* 26, 239-248.
- 537 Theye, T., Reinhardt, J., Goffè, B., Jolivet, L., Brunet, C., 1997. Fe- and Mg-carpholite
538 from the Monte Argentario (Italy): first evidence for high-pressure meta-
539 morphism of the metasedimentary Verrucano sequence, and significance for P-T
540 path reconstruction. *Eur. Journ. Miner.* 9, 859-873.
- 541 Tindle, A.G., Webb, P.C., 1994. Probe-AMPH—A spreadsheet program to classify
542 microprobe-derived amphibole analyses. *Computers & Geosciences* 20, 1201-
543 1228.
- 544 Tsujimori, T., Ernst, W.G., 2013. Lawsonite blueschists and lawsonite eclogites as
545 proxies for palaeo-subduction zone processes: a review. *J. Metam. Geol.*
546 doi:10.1111/jmg.12057.
- 547 Trevisan, L., 1950. L'Elba orientale e la sua tettonica di scivolamento per gravità.
548 *Mem. Ist. Geol. Univ. Padova* 16, 1-30.
- 549 Wei, C.J., Clarke, G.L., 2011. Calculated phase equilibria for MORB compositions: a
550 reappraisal of the metamorphic evolution of lawsonite eclogite. *J. met. Geol.* 29,
551 939-952.
- 552 Westerman, D.S., Dini, A., Innocenti, F., Rocchi, S., 2004. Rise and fall of a nested
553 Christmas-tree laccolith complex, Elba Island, Italy. In: Breitkreuz, C., Petford, N.
554 (Eds): *Physical Geology of High-Level Magmatic Systems*. Geol. Soc. London,
555 *Spec. Publ.* 234, 195-213.
- 556 Winchester, J.A., Floyd, P.A., 1977. Geochemical discrimination of different magma
557 series and their differentiation products using immobile elements. *Chem. Geol.*
558 20, 325-343.
- 559 Zhang, Z.C., Mao, J.W., Saunders, A.D., Ai, Y., Li, Y., Zhao, L., 2009. Petrogenetic
560 modeling of three mafic-ultramafic layered intrusions in the Emeishan large

561 igneous province, SW China, based on isotopic and bulk chemical constraints.
562 Lithos 113, 369-392.

563

564

565

566 **CAPTIONS**

567

568 Figure 1 - Structural sketch map of Tuscany (inner Northern Apennines) with location
569 of the HP-LT mineralogical assemblages in metabasite (black circle) and other
570 rock types (metasediments). The P-T values from Rio Marina (no.11) are
571 presented in this paper; other data Kligfield et al. (1986); Theye et al. (1997);
572 Giorgetti et al. (1998); Rossetti et al. (1999); Brunet et al. (2000); Rossetti et
573 al. (2001); Elter and Pandeli, (2001); Brogi and Giorgetti (2012).

574

575 Figure 2 - Geological sketch map of the Elba Island. The relationships between the
576 tectonic units are highlighted as described in the text. The location of the
577 phengite -and glaucophane-bearing rocks is also indicated.

578

579 Figure 3 - Tectono-stratigraphic columns showing the seven tectonic units belonging
580 both to continental and oceanic environments and forming the tectonic pile of the
581 Elba Island. From right to left, and from the bottom in each column: oceanic unit
582 3: b Σ = Breccia of ophiolitic rocks; LC = limestone and shale (Palombini Shales
583 Fm); C = shale (Varicoloured shales Fm); S = sandstone and shale (Ghiaiето
584 Sandstones Fm); Sc = sandstone and marlstone (Marina di Campo Fm); Ts =
585 shale with limestone and marlstone (Colle Reciso Fm). Oceanic unit 2: Σ =
586 ophiolite; J = radiolarite (Mt. Alpe Cherts Fm); Cl = calcilutite and cherty
587 limestone (Nisportino Fm); L = cherty limestone (Calpionella Limestones Fm); LC

588 = limestone and shale (Palombini Shales Fm). Continental unit 4: Ev =
589 Evaporite (Calcare Cavernoso Fm); M = massive and cherty limestone and
590 dolostone (Pania di Corfino Fm, Mt. Cetona Fm, Calcare Massiccio Fm, Grotta
591 Giusti Limestones, Rosso Ammonitico Fm, Limano cherty Limestones Fms); Mp=
592 marls (Posidonia Marlstones Fm); MI = varicolored shales (Cavo Fm). Continental
593 unit 3: Bphy = black phyllite (Rio Marina Fm); Q = quartzite and phyllite
594 (Verruca Fm, Mt. Serra quartzite Fm); M = marble (Valle Giove Limestones Fm;
595 Capo Pero Limestone Fm; Capo Castello Calcschists Fm); Mc = cherty marble; Cs
596 = calcschist and phyllite (Varicoloured Sericitic Schist Fm); Ms = metasandstone
597 and phyllite (Pseudomacigno Fm). Continental unit 2: P = porphyroids, quartzite
598 and phyllite (Ortano Unit); Q = quartzite; M = massive and cherty limestone and
599 dolostone (Valdana marble Fm); Mp = marls (Posidonia Marlstones Fm); J =
600 radiolarite; Phy = calcschist with interbedded metabasite (Mb) and phyllite
601 (Acquadolce Unit). Oceanic unit 1: Σ = ophiolite. Continental unit 1: Mc =
602 micaschist (Mt. Calamita Fm); Q = quartzite and phyllite (Quarziti di Barabarca
603 Fm); M = dolostone (Crystalline dolostone and dolomitic limestone Fm).
604 Formational names after Bortolotti et al. (2001) and Garfagnoli et al. (2005). The
605 stars indicate the location of the analysed samples.

606

607 Figure 4 - Geological map and cross sections of the Rio Marina area.

608

609 Figure 5 - A) panoramic view of the sampling area; B) lenses of metabasite embedded
610 in calcshist; C) metabasites lenses located mainly along the main schistosity,
611 gently NW-dipping; D) detail of metabasite lens; E-H) metabasite laterally
612 segmented at different scales indicating the pervasiveness of the deformation; I)
613 rock fabric characterized by the presence of porphyroclasts of mafic minerals
614 within a chloritic matrix.

615

616 Figure 6 - A-B) tight and isoclinal folds with $\approx 304/30$ plunging hinge lines deforming
617 the main foliation in calcschists; C) stretching lineation well defined by
618 elongated calcite crystals, NW-SE trending; D) SEM-BSE (scanning electron
619 microscopy-back scattered electron) image showing the textural characteristics
620 and paragenesis of micaschists. Mineral abbreviations after after Kretz (1983)
621 and Bucher and Frey (1994). D) SEM-BSE (scanning electron microscopy-back
622 scattered electron) image showing the textural characteristics and paragenesis of
623 micaschists. Mineral abbreviations after after Kretz (1983) and Bucher and Frey
624 (1994).

625

626 Figure 7 - Immobile elements TAS proxy diagram (Pearce, 2014). Grey area indicates
627 the field of ophiolitic lavas from Troodos (Cyprus) and Semail (Oman) as
628 reported by Pearce (2014). The metabasite under study (white circles) in
629 comparison to Troodos and Semail lavas show a more pronounced alkaline
630 affinity.

631

632 Figure 8 - Micrographs of a metabasite sample (plane polarised light in A-E and
633 crossed polars in F). A) Rounded porphyroclast of clinopyroxene with strain
634 shadow filled by glaucophane; B) Stretched and fractured porphyroclast of
635 clinopyroxene. Fracture is filled by glaucophane fibres grown parallel to the
636 stretching direction; C) Elongated well-developed glaucophane crystals, mostly
637 oriented along the main foliation between clinopyroxene porphyroclasts; D)
638 Glaucophane fibres wrapping around porphyroclasts of clinopyroxene; E) Rock
639 portion affected by retrogression in greenschist facies as shown by the
640 widespread chlorite and by the corona of sphene around ilmenite; F) Late calcite

641 vein cross-cutting at high angle the main foliation. Mineral symbols from Kretz
642 (1983).

643

644 Figure 9 - A) Classification diagram of Na-Amphiboles in metabasite (after Leake et
645 al., 1997). B) Classification diagram for Ca-Na pyroxenes in the metabasite
646 according to Morimoto et al. (1988); $Q = \text{wollastonite} + \text{enstatite} + \text{Ferrosilite}$. C)
647 Classification diagram for Ca-Fe-Mg pyroxenes in the metabasite by Morimoto et
648 al. (1988).

649

650 Figure 10 - P-T diagram showing approximate metamorphic conditions (circles) for the
651 Elba Island blueschists constrained by mineral assemblage and composition of
652 omphacite (yellow) and glaucophane (lilac). X_{Jd} isopleth calculated with the aid of
653 the Sturm (2002) software on the basis of $Ab = Jd + Qtz$ equilibrium calibrated
654 by Holland (1980). X_{Gln} isopleth from calibration by Maruyama et al. (1986).
655 Subfacies boundaries by Tsujimori and Ernst (2013) and some relevant equilibria
656 have been shown. Metamorphic facies and sub-facies abbreviations: L-Bs =
657 lawsonite blueschist; E-Bs = epidote blueschist; Gs = greenschist; E-Am =
658 epidote - amphibolite; Am = amphibolite; Amph-Ec = amphibole eclogite.
659 Mineral stability boundary and equilibria: Gln-in = stability boundary of
660 glaucophane by Maresch (1977); Omph-in = stability boundary of omphacite-in a
661 jadeite-enriched MORB (MORB+ in Tsujimori and Ernst, 2013); $Ab = Jd + Qtz$ by
662 Tsujimori and Ernst (2013); $Lws = An + H_2O$ by Crawford and Fyfe (1965).
663 Mineral abbreviations according to Kretz (1983).

664

665 Figure 11 - SEM-BSE (scanning electron microscopy-back scattered electron) images:
666 A) RMT3 metabasite sample with glaucophane (Gln), clinopyroxene (Cpx) and

667 phengite (Phe). B) Phengite (Phn) from Torre Giove quartzite; phengite is more
668 celadonite -rich in the rim (lighter color).

669

670 Table 1 - XRF analyses of three metabasites samples.

671

672 Table 2 - Representative analyses of Metabasite (sample C19). Beam width was
673 approximately of 1 μm . Table 2. Mineral abbreviations according to Kretz (1983)
674 and Bucher and Frey (1994): Gln=glaucophane; Act=actionolite;
675 Omph=omphacite; Agt=aegirine-augite; Di=diopside; Aug=augite;
676 Clz=clinozoisite; Ps=pistacite. Analyses were performed on the JEOL 8200
677 microprobe, at the University of Milan, operating in WDS/EDS with an
678 accelerating voltage of 15 kV and 5 nA current. Beam width was approximately
679 of 1 μm .

680

681 Table 3 - Selected SEM/EDS analyses of phengites in metabasite (sample RMT3) and
682 quartzite (RIO6B). Analyses were performed on the Philips XL30 SEM at the
683 University of Siena, operating in EDS/EDAX with an accelerating voltage of 20
684 kV.

685

686

687

finding of HP-LT metamorphism in Elba Island

implications for the geodynamic evolution of N.Apennines

revision of the tectonic units involved in the N.Appennine stacking

Table1

	C19	RMT2	RMT3
wt. %			
SiO ₂	44.84	43.60	44.15
TiO ₂	1.15	0.84	1.03
Al ₂ O ₃	17.04	13.72	15.23
FeO _t	10.52	7.96	9.45
MnO	0.16	0.09	0.12
MgO	9.92	7.29	9.55
CaO	6.28	12.36	9.80
Na ₂ O	2.10	3.49	3.11
K ₂ O	0.58	1.04	0.59
P ₂ O ₅	0.14	0.13	0.14
L.O.I.	6.86	9.25	6.68
Tot	99.58	99.75	99.85
ppm			
Ni	139	91	133
Cr	287	199	265
V	193	111	157
Rb	40	46	26
Sr	234	483	445
Ba	21	104	46
Y	24	17	22
Zr	106	91	105
Nb	8	7	7
La	23	7	10
Ce	70	27	38

Table2

	<u>Amphiboles</u>		<u>Clinopyroxenes</u>				<u>Feldspars</u>		<u>Epidotes</u>		<u>Chlorite</u>
	Gln	Act	Omph	Agt	Di	Aug	Ab	An	Clz	Ps	
wt. %											
SiO ₂	58.08	57.28	55.20	54.00	51.63	52.13	68.36	42.51	39.27	37.87	30.03
TiO ₂	0.22	0.03	0.10	0.01	1.00	0.03	0.01	0.01	0.12	0.06	0.02
Al ₂ O ₃	9.63	1.06	7.20	3.26	2.15	4.44	19.50	36.79	32.55	22.28	20.74
Cr ₂ O ₃		0.04	0.28	0.19	0.02				0.02	0.09	0.03
FeO _t	9.76	6.89	9.36	9.86	6.71	13.69	0.07	0.17	1.4	12.55	14.26
MnO	0.17	0.30	0.13	0.23	0.19	0.22			0.03	0.11	0.38
MgO	10.56	18.47	7.44	9.90	15.04	14.23	0.01	0.01	0.06	0.03	20.97
CaO	1.09	11.20	11.65	15.19	21.64	13.22	0.03	19.80	23.55	22.18	0.06
Na ₂ O	6.16	0.86	7.34	5.33	0.36	0.35	11.68	0.05	0.01	0.03	0.01
K ₂ O	0.02	0.03	0.04	0.04	0.03	0.11			0.01	0.02	0.08
Tot	95.68	96.14	98.74	98.01	98.76	98.42	99.66	99.37	97.02	95.22	86.58
ΣO	23	23	6	6	6	6.066	8	8	25	25	28
Si	8.063	8.087	2.011	2.004	1.929	1.982	2.994	1.982	6.027	6.320	5.986
Al ^{IV}					0.071	0.018	1.008	2.024			2.014
Al ^{VI}	1.576	0.176	0.309	0.143	0.024	0.181			5.895	4.387	2.864
Ti	0.022	0.004	0.003		0.028	0.001			0.014	0.008	0.003
Cr		0.004	0.008	0.006	0.001				0.002	0.012	0.005
Fe	1.133	0.813	0.289	0.306	0.210	0.435	0.003	0.007	0.180	1.751	2.377
Mn	0.020	0.036	0.004	0.007	0.006	0.007			0.004	0.016	0.064
Mg	2.190	3.885	0.404	0.558	0.838	0.806	0.001	0.001	0.014	0.007	6.231
Ca	0.163	1.693	0.455	0.604	0.866	0.538	0.001	0.989	3.872	3.966	0.013
Na	1.658	0.234	0.519	0.391	0.026	0.026	0.992	0.005	0.003	0.010	0.004
K	0.003	0.005	0.002	0.002	0.001	0.005		0.002	0.002	0.004	0.020
Fe ³⁺	0.266	0.024	0.175	0.227	0.017						
Fe ²⁺	0.867	0.789	0.110	0.079	0.193	0.435					
ΣCat	14.827	14.938	4.000	4.000	4.000	4.000	4.998	5.009	16.013	16.480	19.581
X _{Gln}	0.86										
X _{Jd}			0.33	0.15							
X _{Wo}					0.45	0.30					
X _{En}					0.47	0.45					
X _{Fs}					0.11	0.25					
X _Q			0.48	0.62							
X _{Ae}			0.19	0.24							
X _{Ps}									0.09	0.82	
X _{An}							0.00	1.00			
X _{Ab}							1.00	0.00			
X _{Mg}	0.72	0.83	0.70	0.88	0.81	0.65					

Table3

	Metabasite RMT3	Quartzite RIO6A
wt. %		
SiO ₂	52.69	51.65
TiO ₂	0.15	0.19
Al ₂ O ₃	24.61	23.77
FeO _t	3.34	5.93
MnO	0.12	0.11
MgO	4.97	2.98
CaO	0.18	0.11
Na ₂ O	0.12	0.08
K ₂ O	9.66	10.96
Tot	95.85	95.77
ΣO	11	11
Si	3.49	3.50
Al ^{IV}	0.50	0.50
Al ^{VI}	1.42	1.40
Ti	0.01	0.01
Fe	0.19	0.34
Mn	0.00	0.00
Mg	0.49	0.30
Ca	0.01	0.01
Na	0.01	0.01
K	0.81	0.94
ΣCat	6.95	7.02
X _{Cel}	0.50	0.50

Figure3
[Click here to download high resolution image](#)

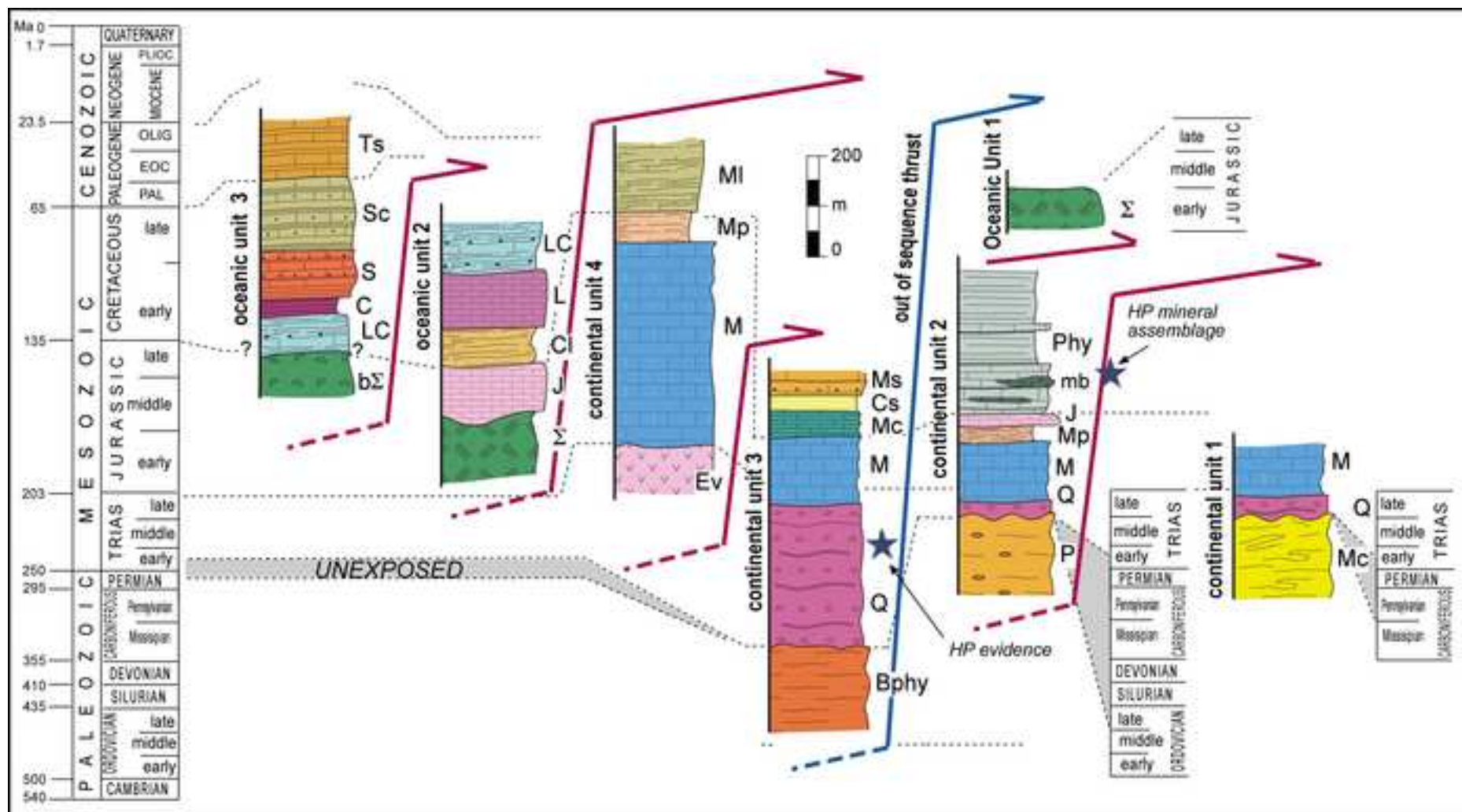


FIGURE 3

Figure4

[Click here to download high resolution image](#)

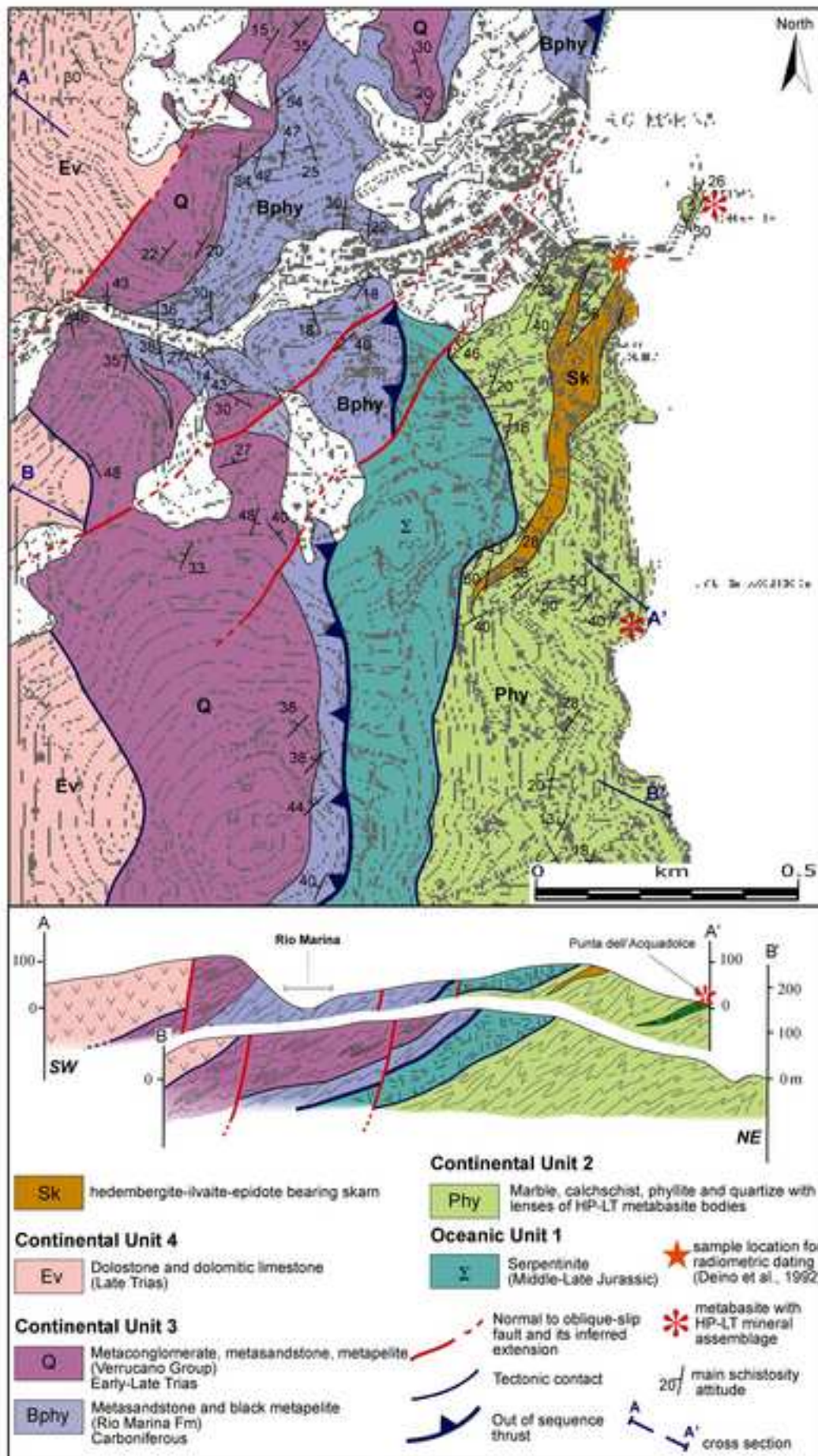


FIGURE 4

Figure5
[Click here to download high resolution image](#)

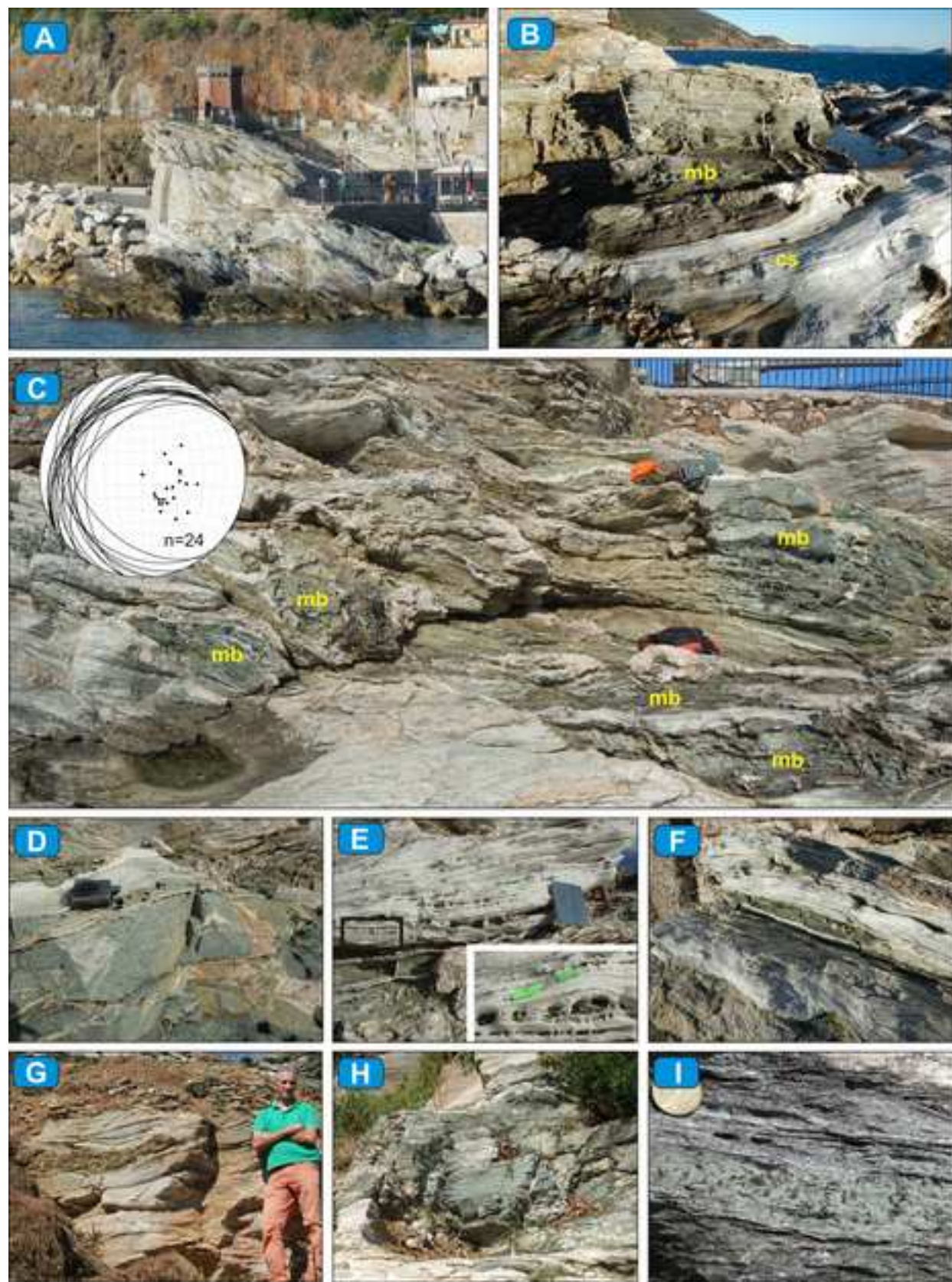


FIGURE 5

Figure6
[Click here to download high resolution image](#)

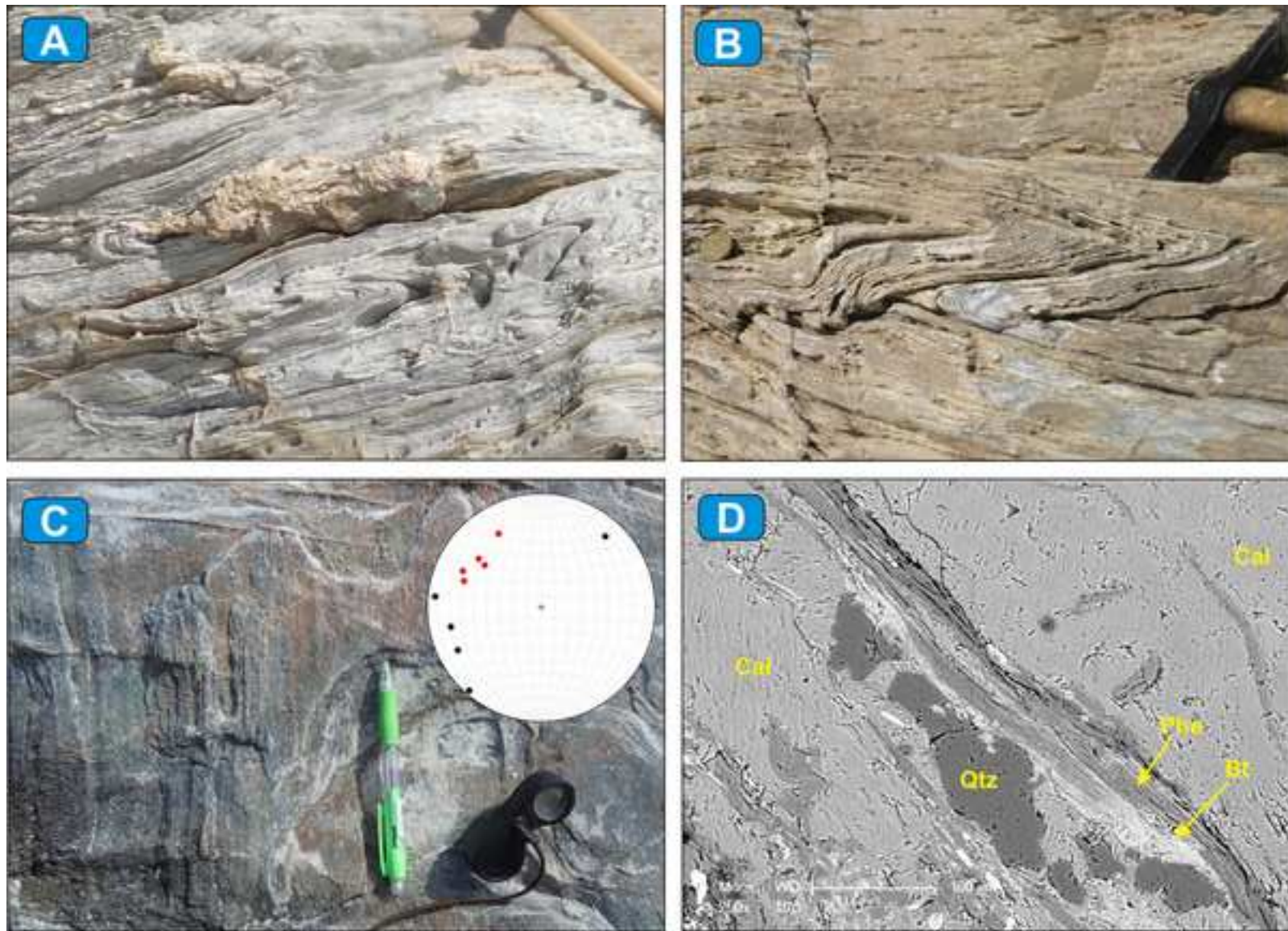


FIGURE 6

Figure7
[Click here to download high resolution image](#)

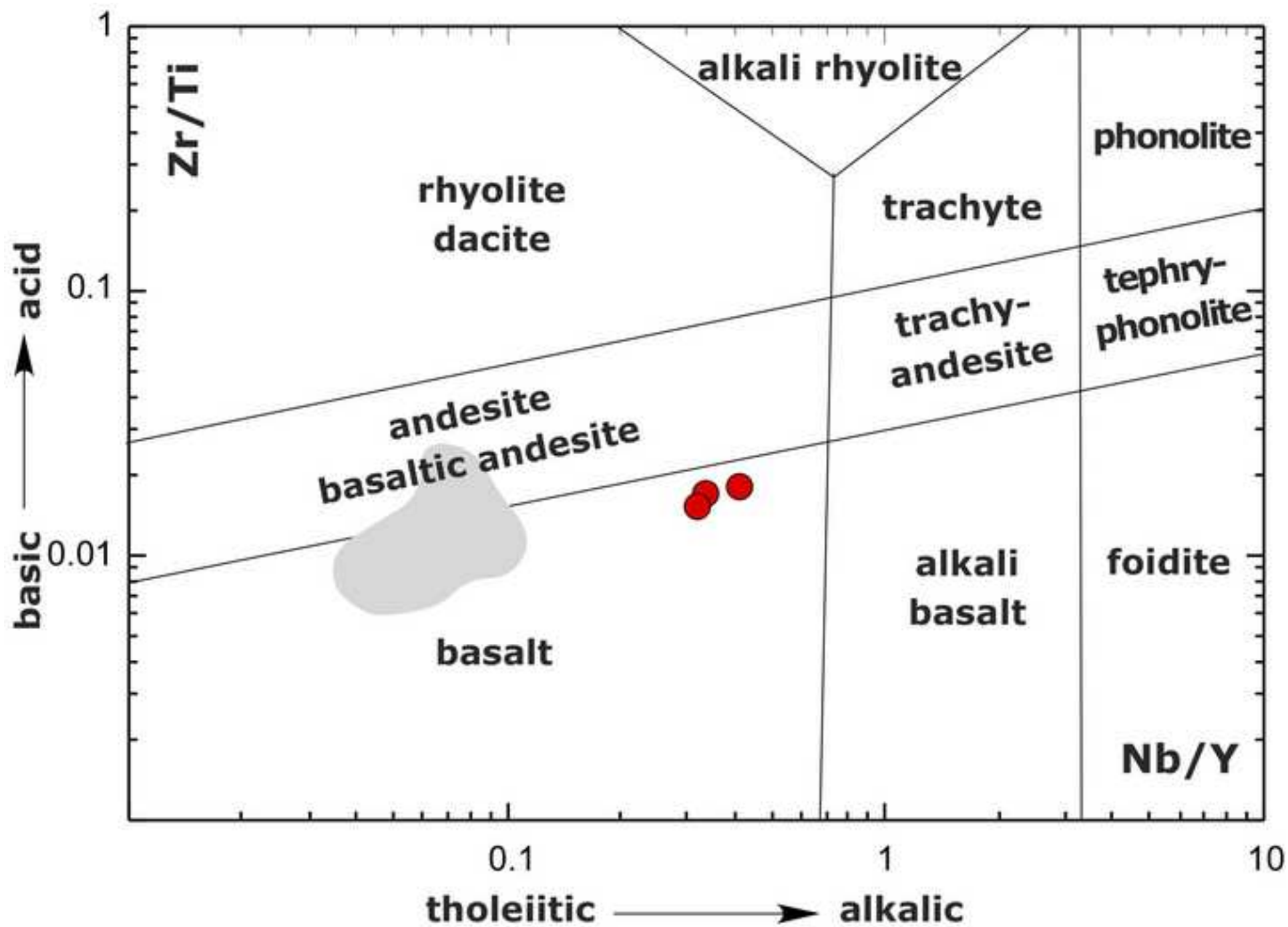


Figure8
[Click here to download high resolution image](#)

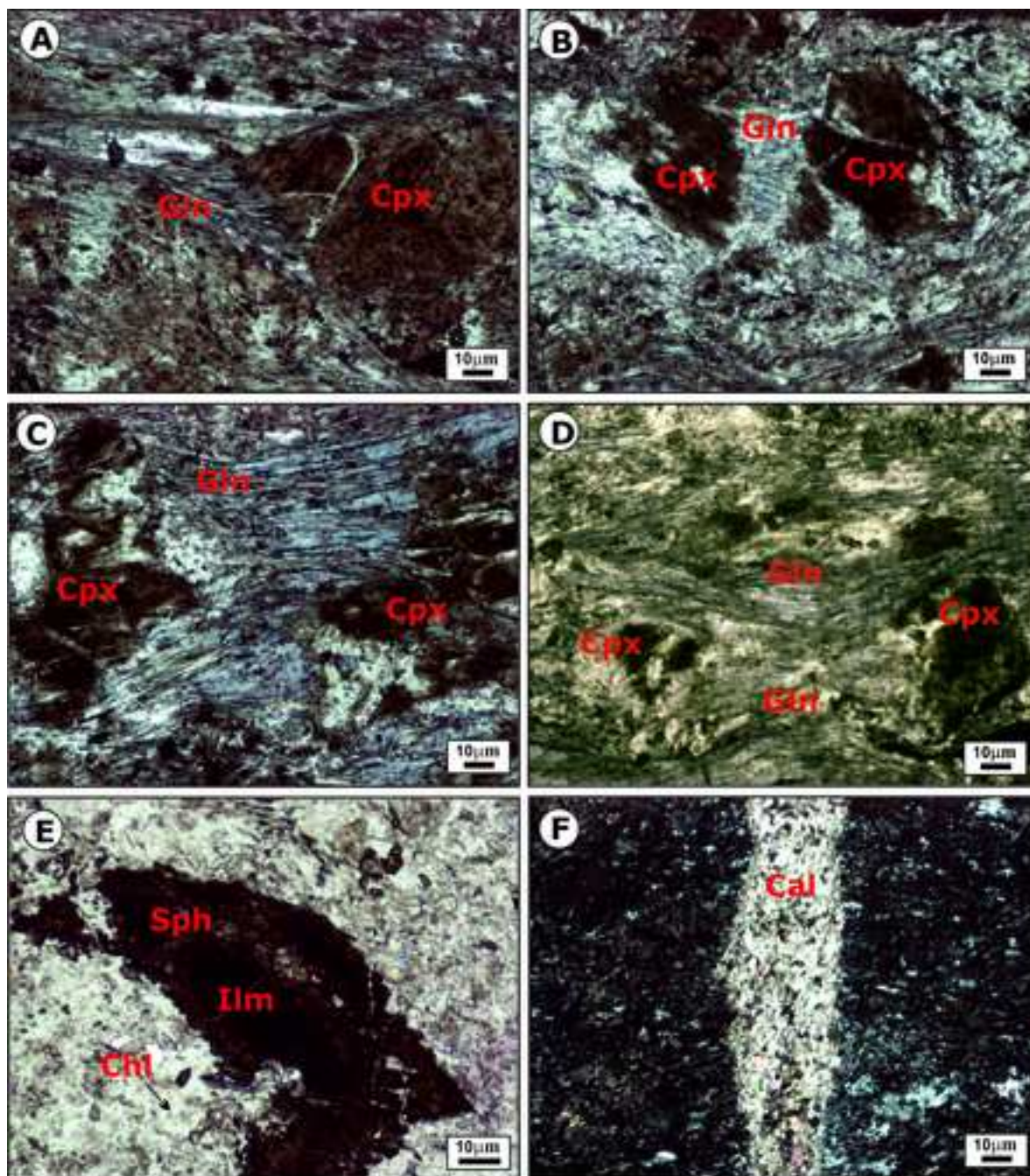


FIGURE 8

Figure9
[Click here to download high resolution image](#)

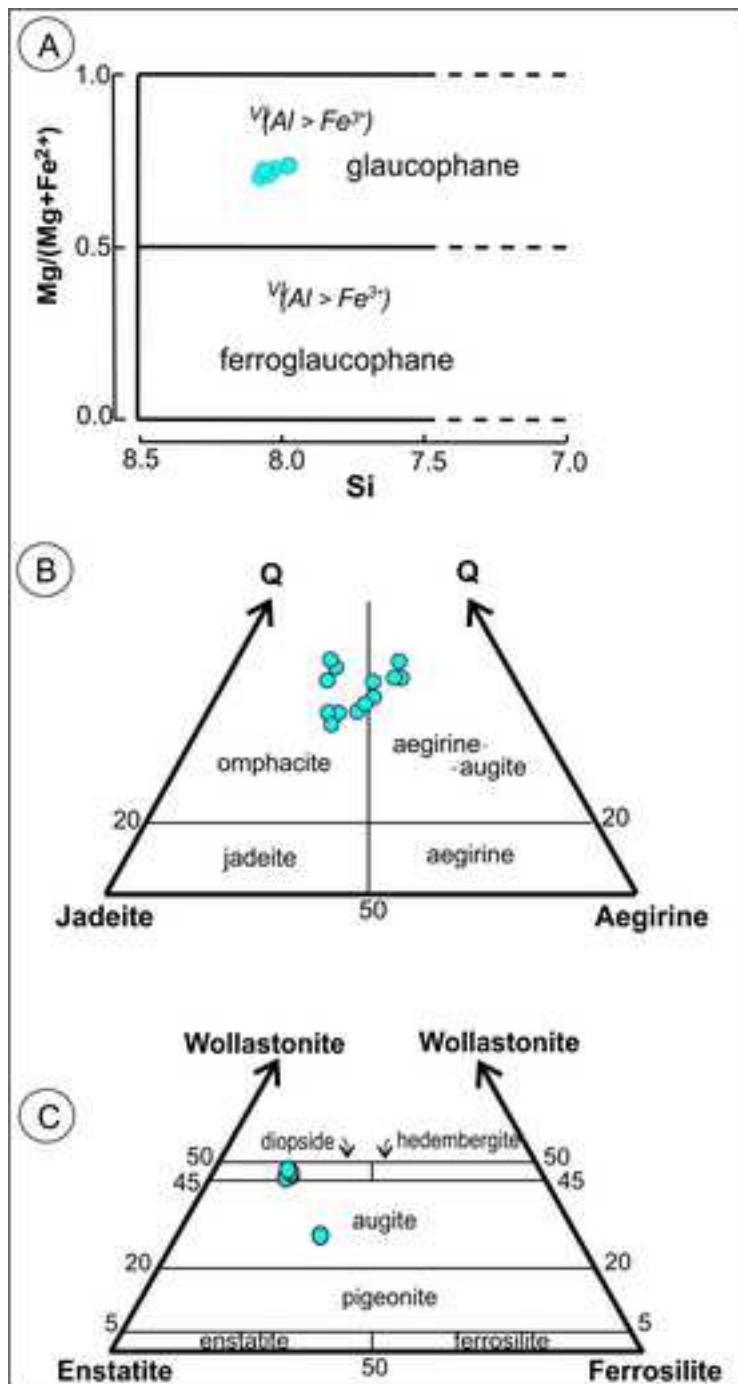


FIGURE 9

Figure10
[Click here to download high resolution image](#)

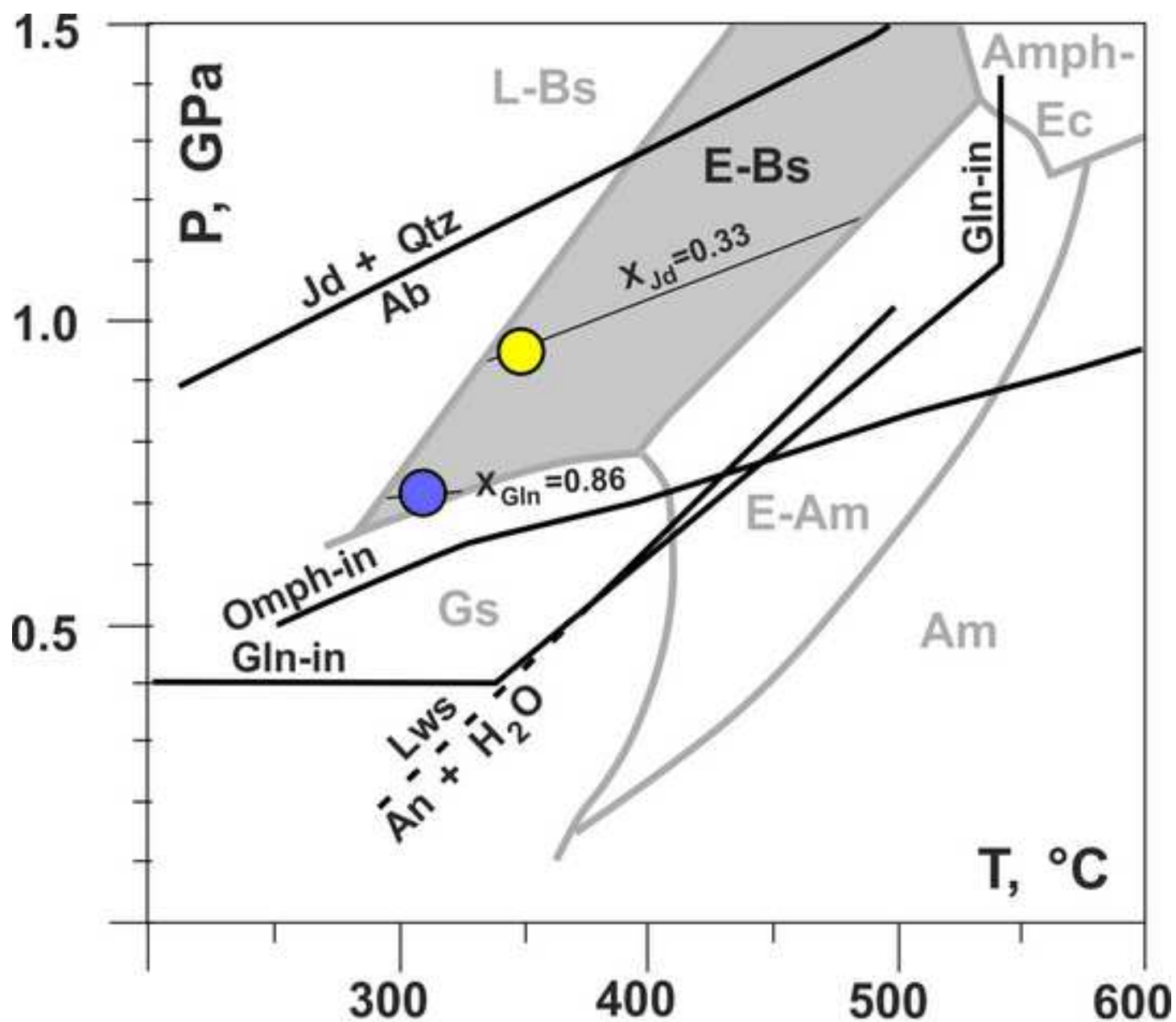


FIGURE 10

Figure11

[Click here to download high resolution image](#)

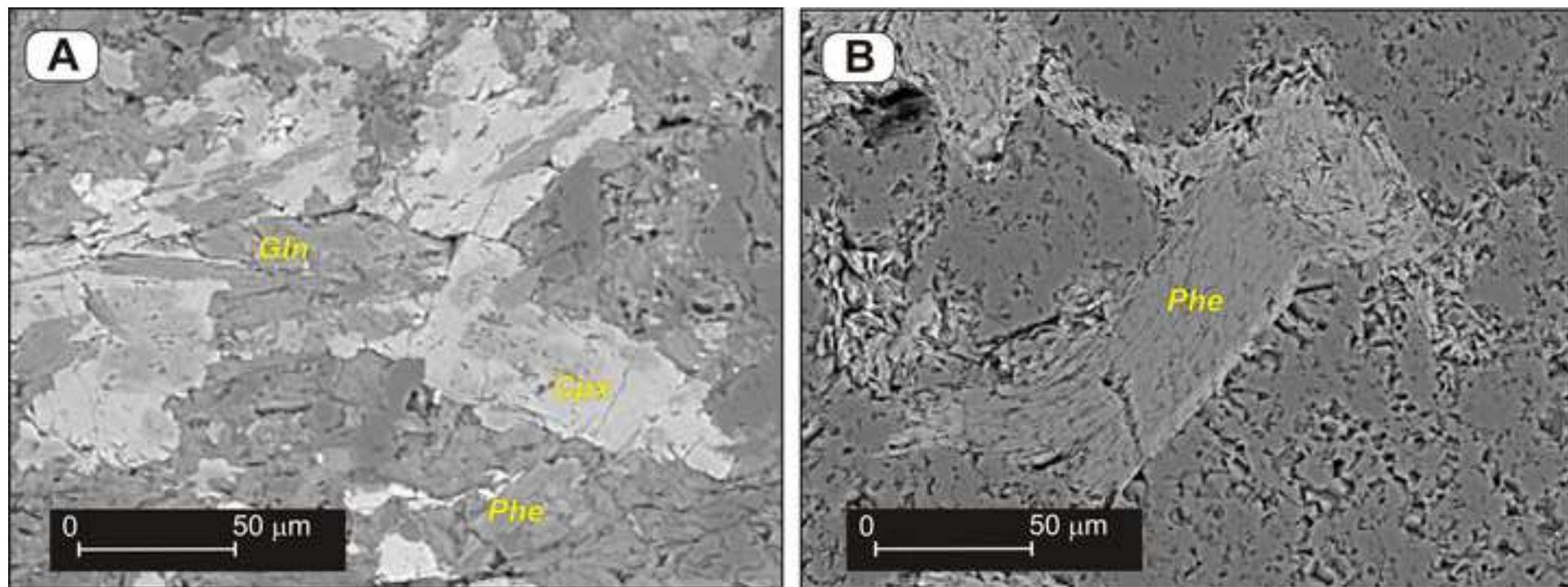


FIGURE 11